

Synthesize and Optical properties of ZnO: Eu Microspheres Based Nano-sheets at Direct and Indirect Excitation

M. Najafi* and H. Haratizadeh

Department of Physics, Shahrood University, Shahrood, I. R. Iran.

(* Corresponding author: najafi@shahroodut.ac.ir
(Received: 28 Oct 2014 and Accepted: 22 Feb. 2015)

Abstract

Europium (Eu) doped ZnO microsphere based nano-sheets were synthesized through hydrothermal method. Effects of different concentrations of Europium on structural and optical properties of ZnO nano-sheets were investigated in detail. Prepared un-doped and Eu-doped ZnO samples were characterized using X-Ray diffraction (XRD), energy dispersive X-ray spectroscopy (EDX), scanning electron microscopy (SEM), diffuse reflectance spectroscopy (DRS) and Photoluminescence (PL) spectroscopy at fluorescence and phosphorescence modes. Results for XRD and EDX showed Eu ions were successfully incorporated into ZnO nanostructures. Fluorescence Spectroscopy indicated that indirect excitation of Eu ions was more effective than direct excitation, which is attributed to an efficient absorption process at UV wavelengths in ZnO host and energy transfer from photon generated electron-hole pair in the ZnO nano-sheets to Eu ions at indirect excitations. Phosphorescence spectroscopy also showed a sharp red luminescence from intra 4f transitions of Eu^{3+} ions at excitation wavelengths of 395nm and 464nm which was consistent with XRD and EDX results

Keywords: Hydrothermal, Photoluminescence, Nano-sheets, ZnO.

1. INTRODUCTION

Many investigations have been accomplished on development of synthesizing new materials based on ZnO with low-cost and new morphologies to enhance optical, magnetic and electrical properties [1-2]. ZnO is a wide band-gap (3.37eV) II-VI compound semiconductor with high excitation binding energy (60meV) at room temperature which made it a promising candidate for optoelectronic applications. ZnO exhibits emission from near UV to visible blue-green region, which are attributed to band edge transition and intrinsic defects emissions of ZnO, respectively [3]. Besides, it is a potential candidate as a suitable host lattice for doping several luminescence centers of

various rare-earth(RE) ions due to wide band gap energy of ZnO [4-5]. RE ions are unique dopants, because they are optically and magnetically active in the semiconductor host crystals [6]. Also, RE ions are good luminescence centers due to their narrow and intense emission lines originate from the 4f-4f transitions. Among the RE ions, Eu^{3+} ions have been extensively studied due to their red-light emission [7]. The red emission of Eu^{3+} ions, which is a result of 4f-shell transitions, occurs from the excited level down to the lower levels: ${}^5\text{D}_0$ - ${}^7\text{F}_J$ ($J=0, 1, 2, 3$)[8-9].

The different procedures which have been used frequently for ZnO doped rare earth ions have made a great influence on their

morphology and optical properties. Therefore, several efforts have been made to prepare various ZnO: Eu nano structures, including nanowires[10-12], nanorods[13-15], nanobelts[16-17] and nanodisks[18], which have been fabricated by different methods such as sol-gel[19], micro-emulsion method[5,20], spray pyrolysis[21] and electric deposition[22]. Compared to these methods, hydrothermal method is very simple and has some advantages specifically such as low environment temperature, large-scale production, uniform size and good dispersion of dopant. Recently, Nano-sheets as a new class of nanostructured materials have got attentions due to their high anisotropy and nanometer-scale thickness which bring them interesting properties [23-25]. There are limited reports around successfully incorporated Eu^{3+} ions into ZnO nano-sheets by hydrothermal method. Besides, the role of local environment and symmetry of ions in host lattice and their effect on red luminescence is still in ambiguity. Therefore, more information is required for developing ZnO:Eu with enhanced red luminescence to extend its application in different fields.

In this study, Eu^{3+} doped ZnO microspheres based nano-sheets with different concentrations of Eu were prepared through hydrothermal method. Photoluminescence spectra of Eu^{3+} doped ZnO nano-sheets were discussed systematically. In addition, energy transfer mechanism was discussed through Fluorescence and phosphorescence spectra of Eu^{3+} doped ZnO nano-sheets. Furthermore, the effects of concentration of Eu^{3+} ions on structural and optical properties of ZnO nano-sheets were investigated in detail.

2. EXPERIMENTAL

2.1. Materials

All chemicals were purchased from Merck and Aldrich companies with analytic grade reagents and without any further purification.

2.2. Synthesis of Eu^{3+} doped ZnO microspheres

The ZnO: Eu samples were fabricated through hydrothermal Method. Chemical synthesis of europium doped zinc oxide microspheres was carried out in water as a medium. Zinc nitrate and europium nitrate salts were also used as precursors. Firstly, $\text{Zn}(\text{NO}_3)_2 \cdot 6\text{H}_2\text{O}$ (99.9%) and then a solution of urea($(\text{NH}_2)_2 \text{CO}$) were added to the above solution under stirring. The 2.5mol%, 5mol%, 10mol% and 20mol% europium nitrate were distilled in water then added drop wise to form a 50ml solution. Secondly, the mixture was transferred to a Teflon-lined stainless steel autoclave and was heated at 120°C for 6h after stirring for 10min. After the growth, the system was allowed to cool down to room temperature and the product was collected by washing with deionized water and ethanol for several times, separated by centrifugation and then dried in room temperature to obtain the precursor. Finally, Eu-doped ZnO samples with various Eu concentrations were obtained by annealing the precursor at 400°C for 2h in the air.

2.3. Characterization

Crystal structure, quality and phase identification of samples were studied by X-ray diffractometric (XRD) with Ni-filtered $\text{Cu-K}\alpha$ radiation. Morphology of the samples was analyzed by field emission scanning electron microscope (FE-SEM, JEOL JSM-6700F). The elemental composition of the Eu samples was determined using energy dispersive X-ray spectroscopy (EDX, Hitachi S-4700 II). The UV/vis diffuse reflectance spectra of Eu-doped ZnO nanocrystals were measured by a Perkin-Elmer Lambda 900 UV/vis/NIR spectrometer using BaSO_4 as a blank. Room temperature photoluminescence spectra were taken on a Perkin-Elmer LS55 spectrophotometer equipped with a 450W Xe lamp as excitation source.

3. RESULTS AND DISCUSSION

3.1. Structure and morphology characterizations

Figure.1 shows typical XRD patterns of pure and Eu-doped ZnO microspheres with different Eu concentrations. All peaks in the X-ray diffraction pattern were assigned to the typical wurtzite structure of ZnO (JCPDS card no. 36-1451). There were not any diffraction peaks originating from europium or any other impurities in the XRD data. The mean grain size(D) of the samples was determined using Debye–Scherer formula ($D = 0.89\lambda / (\beta \cos\theta)$) [26], where λ is the X-ray wavelength, β is full width at half maximum (FWHM) of the ZnO (101) peak and θ is the diffraction angle. It gives the grain sizes of 18nm, 22.7nm, 23.5nm, 27nm and 28.5nm for undoped and doped ZnO with 2.5 mol%, 5 mol%, 10 mol% and 20 mol% Eu concentrations, respectively. Increasing in grain size of Eu-doped ZnO samples by increase of Eu concentration is attributed to larger covalent radius of Eu^{3+} ions (0.96\AA) rather than Zn^{2+} ions (0.6\AA). Furthermore, it can be seen that the positions of the main diffraction peaks were shifted to low-angle with increase of Eu concentrations. This shift of diffraction angles indicates that Eu^{3+} ions have been successfully doped into the crystal lattice of ZnO host. These phenomena could also be explained in terms of the larger covalent radius of Eu^{3+} ions rather than Zn^{2+} ions. The Eu^{3+} ions doped into the ZnO matrix caused expansion of the unit-cell volume of the ZnO:Eu nano crystals, resulting in tensile stresses which caused the XRD peaks were shifted to lower angles[27]. In addition, the decrease of diffraction peaks indicates that the crystallization of samples became worse with the increase of Eu concentration due to formation of stresses by the difference in ion size between zinc and Europium ions.

In the synthesis of Eu-doped ZnO microspheres, successful doping of Eu^{3+} ions into the ZnO lattice could be confirmed

by EDX analysis. EDX results show that elemental ratio of Eu ions to Zn ions incorporated in the Eu-doped ZnO samples were 0.05, 0.1, 0.2 and 0.4 for 2.5 mol%, 5 mol%, 10 mol% and 20 mol% $\text{Eu}(\text{NO}_3)_3$ used in the precursor solution, respectively. Figure 2 shows the schematic pattern of EDX results for each sample. It is clear that by increasing the Eu concentration the elemental percentages of Eu incorporated ions into the ZnO lattice were increased.

Figure 3 shows SEM images of un-doped ZnO and 20 mol% Eu-doped ZnO microspheres based nano-sheets with diameters within 10-30 μm synthesized through hydrothermal method. Figure 3a and b (with different scale of magnification) show low magnification SEM images of ZnO and ZnO:Eu, respectively. High-magnification SEM images of samples in figure 3c and d show microspheres were constructed by nano-sheets with thickness of 5-25nm. Figure 3d also shows the ZnO morphology was influenced by Eu doping.

3.2. UV-Vis spectroscopy

Figure 4 represents the diffuse reflectance spectra of Eu^{3+} doped ZnO microspheres with different Eu concentrations. The Eu^{3+} based reflectance graphs show higher reflectance with increase Eu concentration. Moreover, the samples showed absorption edge blue shift with increasing Eu concentration. The observation is attributed to the ‘Burstein-Moss effect’. According to the Moss–Burstein theory, in doped zinc oxide nanostructures, donor electrons occupy states at the bottom of the conduction band. Since the Pauli principle prevents states from being doubly occupied, the valence electrons require extra energy to be excited to higher energy states in the conduction band [28, 29]. In addition, a weak peak centered at 464nm for the 20 mol% Eu doped ZnO sample was observed, which is assigned to the ${}^7\text{F}_0 \rightarrow {}^5\text{D}_2$ transition of Eu^{3+} as usually observed in the diffuse reflectance spectrum of Eu^{3+} .

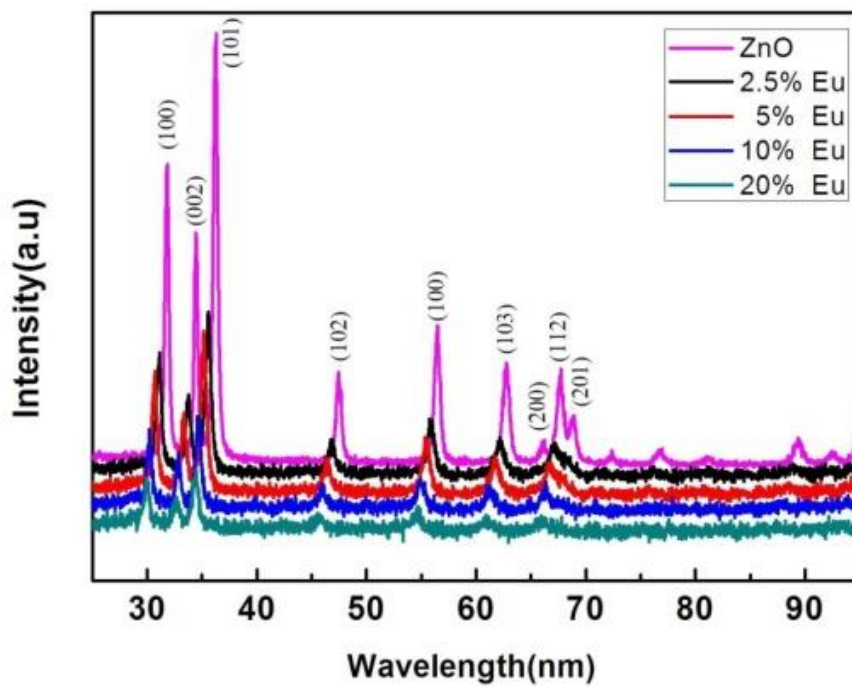


Figure 1. XRD patterns of un-doped and Eu-doped ZnO samples with different Eu concentrations.

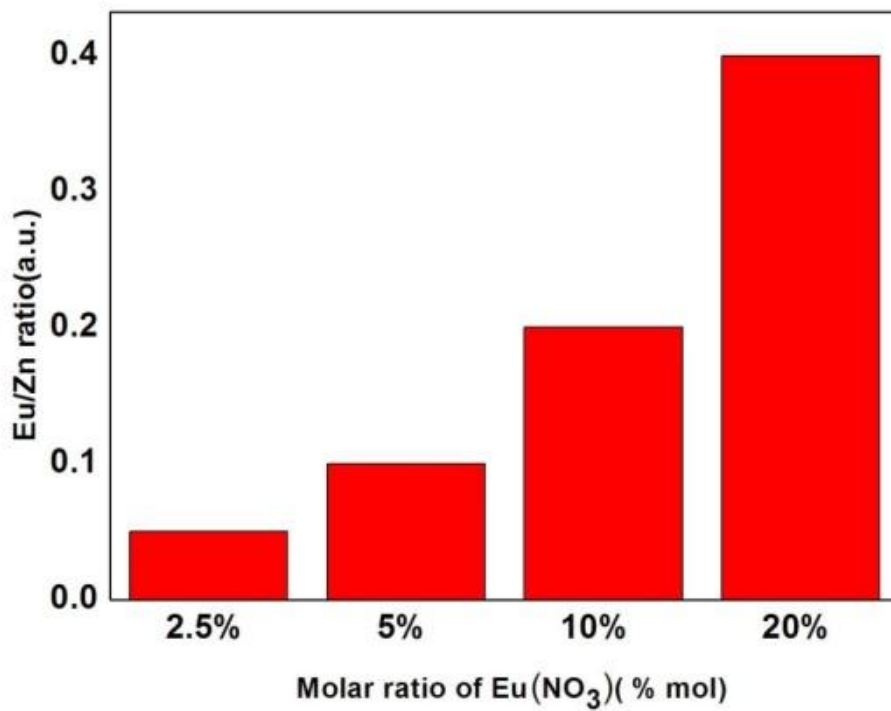


Figure 2. Schematic pattern for EDX of Eu-doped ZnO samples.

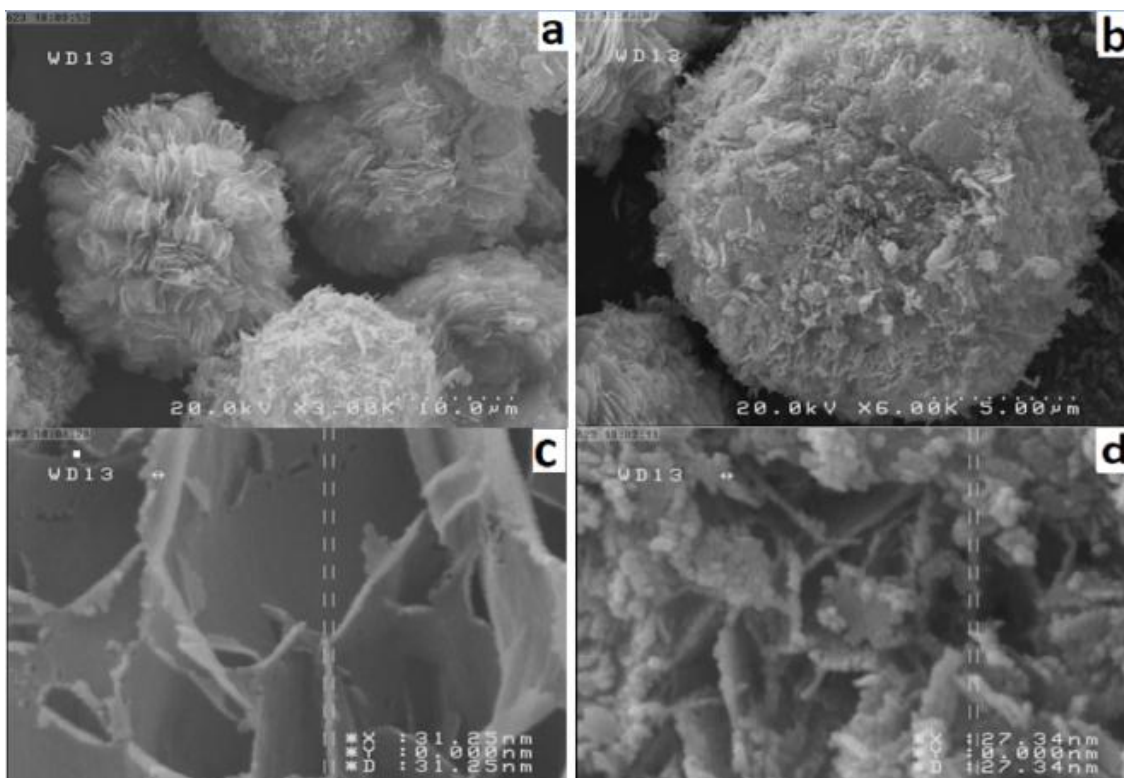


Figure 3. SEM images of un-doped and Eu-doped ZnO microspheres based nanosheets. a) low-magnification images of ZnO, b) low-magnification images of ZnO:Eu, c) high-magnification images of ZnO, d) high-magnification images of ZnO:Eu.

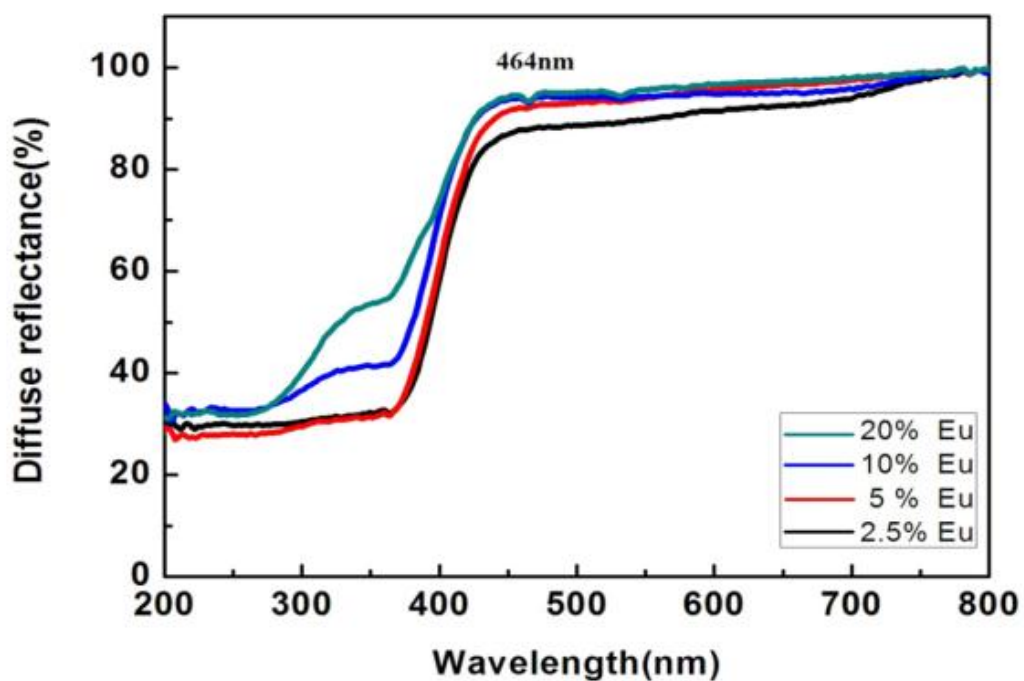


Figure 4. Diffuse reflectance spectra of different Eu-doped ZnO samples.

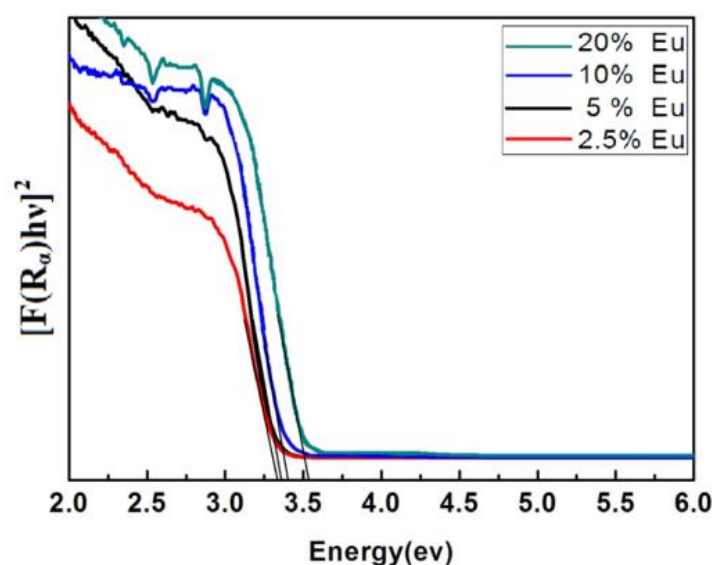


Figure 5. Plot of $[F(R_d)hv]^2$ versus photon energy ($h\nu$) for different Eu-doped ZnO samples.

The band gap of Eu^{3+} doped ZnO samples was calculated from the reflectance study using the Kubelka-Munk relation to convert the reflectance into a Kubelka-Munk function $F(R_d)$, where $F(R_d) = (1 - R_d)^2 / 2R_d$ and R_d is the observed diffuse reflectance in UV/vis spectra [30]. To derive the band gap energies for Eu^{3+} doped ZnO microspheres, $[F(R_d)hv]^2$ was plotted versus photon energy ($h\nu$) (Figure 5). The band gap energy calculated for the 2.5 mol% Eu sample was $3.37 \pm 0.01 \text{ eV}$. It is clear that with increasing Eu concentration the band gap have increased slightly due to excess amounts of Eu concentration.

3.3. Photoluminescence properties

Process of light absorption, which a valence electron is promoted from ground state to vibrational level in the excited singlet manifold, is in order of one femtosecond (10^{-15} s). The excited atom ends up at the lowest vibrational level of conduction band via vibrational relaxation and internal conversion. Vibrational relaxation is very rapid in order of picoseconds (10^{-12} s) or less. Consequently, atoms that are excited to different vibrational energy levels of the same excited electronic state quickly return to the lowest vibrational energy level of the

excited state. Fluorescence process is referred to the emission of a photon from a singlet excited state to a singlet ground state or between any two energy levels with the same spin. Fluorescence decays rapidly after the excitation source is removed as the average lifetime of the electron in the excited state is only $10^{-5} - 10^{-8} \text{ s}$ therefore the probability of a fluorescent transition is very high. In this manner, through intersystem crossing, energy can pass from the ground vibrational energy level of an excited electronic state into a high vibrational energy level with a different spin state via nonradioactive transition. On the other hand, phosphorescence is a process of emission between triplet excited state and a singlet ground state or between any two energy levels that differ in their respective spin states, and as the average lifetime for phosphorescence ranges from 10^{-4} to 10^4 s , phosphorescence may continue for some time after removing the excitation source. Once the atom reaches this state, it will reside for a very long time there (from microseconds to seconds) before it will decay to the ground state. This is due to the spin-forbidden transitions from excited state to ground state. Figure 6 shows the schematic diagram of electron transition of Eu ions and light emitting during

fluorescence and phosphorescence process. The energy levels of the lanthanide's 4f-shell have equal parity, hence electric dipole transitions are forbidden. In a solid, the slight mixing with odd-parity wave functions makes the transition slightly allowed. The absorption and emission cross sections are therefore small, and luminescence lifetime can be quite long(ms). As the long lanthanide luminescence lifetimes are in the microsecond to milisecond time range, so

for better detection of Eu Ions and their effects, besides of fluorescence spectroscopy, we have used phosphorescence emission which its decay time is in the same region of lanthanide luminescence lifetimes. we could subtracted the ZnO spectrum since its emission is in nanosecond region. Therefore, we observe the emission spectrum emerging from lanthanides. Particularly, this method is very useful for weak peak of Eu Ions which has been affected by the broad emission band.

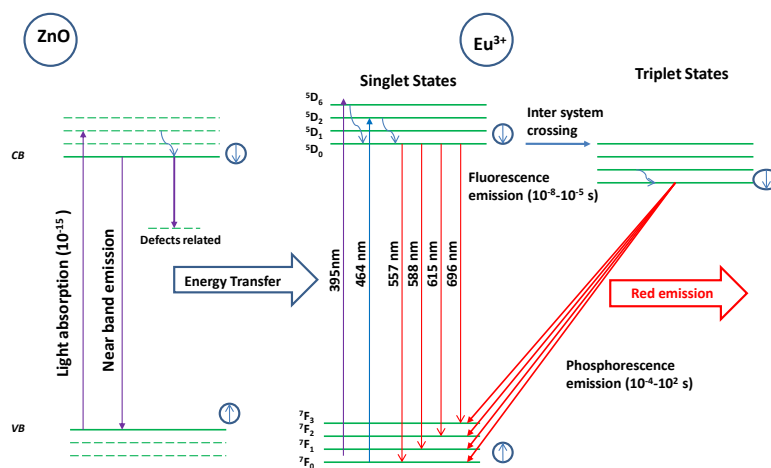


Figure 2. Transition diagram and light emitting during fluorescence and phosphorescence process.

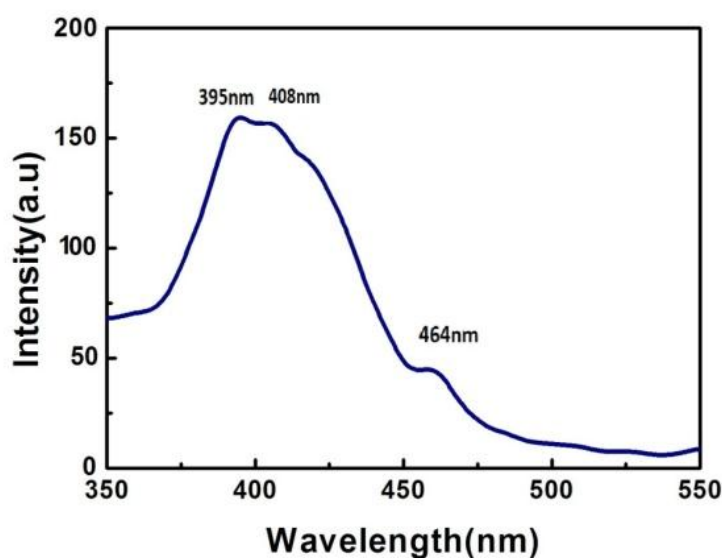


Figure 3. Room temperature fluorescence excitation spectra of ZnO:5mol%Eu³⁺ at 615nm.

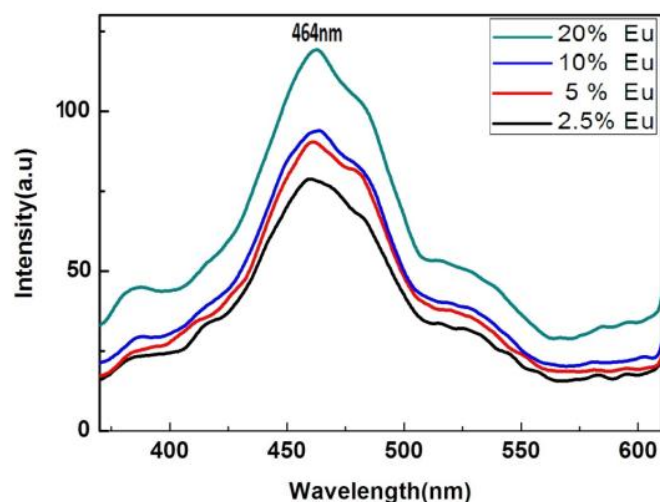


Figure 4. Room temperature fluorescence emission spectra of $\text{ZnO}:\text{Eu}^{3+}$ for various Eu concentrations at indirect excitation at 325nm.

In this work, room temperature photoluminescence (PL) and photoluminescence excitation (PLE) of Eu-doped ZnO microspheres were measured on PerkinElmer LS55 spectro fluorimeter. Figure 7 shows the photoluminescence excitation (PLE) spectra of the 5mol% Eu-doped ZnO microspheres monitored at 615nm. It indicates excitation peaks at 464nm, 408nm and strong excitation peak at 395 nm corresponding to the NBE transition in ZnO, attributed to ${}^7\text{F}_0 \rightarrow {}^5\text{D}_2$, ${}^7\text{F}_0 \rightarrow {}^5\text{D}_3$ and ${}^7\text{F}_0 \rightarrow {}^5\text{L}_6$ transitions of Eu^{3+} ions, respectively.

Figure 8 shows PL spectra Eu-doped ZnO microspheres with different Eu concentrations under excitation at 325nm. It exhibits a UV emission band centered at 395 nm attributed to near band emission (NBE) of ZnO. The broad defect emission centered at 464 nm which is resulted from recombination of photo-generated hole with a singly ionized charge state of intrinsic defects such as oxygen vacancy defect has been observed [31-33]. Energy of broad defect emission of ZnO is close to the photon energy resonantly excited ${}^7\text{F}_0 \rightarrow {}^5\text{D}_2$ transition of Eu^{3+} ions. Therefore, it is obvious that the Eu^{3+} ions absorb the energy through the intrinsic defects of ZnO. In addition, there is a weak peak at around 525

nm in doped Eu ZnO samples which is related to zinc and oxygen vacancy defects [34-36]. Stronger emission peak in 464nm was observed with increasing Eu concentration. Since this wavelength is equal to resonance excitation wavelength of ${}^7\text{F}_0 \rightarrow {}^5\text{D}_2$, we expect more energy transfer from host ZnO to Eu^{3+} ions with increasing Eu concentration.

Figure 9 illustrates the PL spectra under excitation at 395nm, which is consistent with PLE spectra for different concentrations. There were four emission bands peaks at 557, 588, 615 and 696 nm. These emission bands are attributed to the ${}^5\text{D}_0 \rightarrow {}^7\text{F}_j$ ($j=0-3$) transitions of the Eu^{3+} ions, respectively. The energies of the peaks were well matched with the energies of intra4f transitions of Eu^{3+} ions [37]. The peak of ${}^5\text{D}_0 \rightarrow {}^7\text{F}_2$ transition related to 20mol% Eu doped ZnO sample was the strongest peak in comparison with other peaks. ${}^5\text{D}_0 \rightarrow {}^7\text{F}_2$ emission arising from an electric-dipole transition results in a large transition probability in crystal fields with inversion anti-symmetry [38]. In addition ${}^5\text{D}_0 \rightarrow {}^7\text{F}_1$ transition, which originates from a magnetic-dipole transition, indicates that Eu^{3+} ions occupy a site with inversion symmetry. The intensity of ${}^5\text{D}_0 \rightarrow {}^7\text{F}_2$ transition of $\text{ZnO}:\text{Eu}^{3+}$ was stronger than

$^5D_0 \rightarrow ^7F_1$ transition; this result revealed that due to the larger covalent radius, the Eu^{3+} ions located at a site of inversion anti-symmetry in ZnO host. A lower symmetry around Eu^{3+} ion would result in a higher $I(^5D_0 \rightarrow ^7F_2)/I(^5D_0 \rightarrow ^7F_1)$ value, known as an asymmetric factor or asymmetric ratio[39]. Presence of a more intense red peak at 615nm, due to the $^5D_0 \rightarrow ^7F_2$ transition, confirms that Eu^{3+} emission is parity forbidden and observed only when the lattice environment is distorted and contains

non-inversion symmetry [38]. The observation of the red emission under no resonant conditions strongly suggests that there exists energy transfer mechanism between the ZnO host and the Eu^{3+} ions via the defect states [40-41]. It is clear that by increasing Eu concentration broad defect intensity decreased, while Eu intra 4f emissions intensity increased which was due to more energy transfer from ZnO host to Eu^{3+} ions.

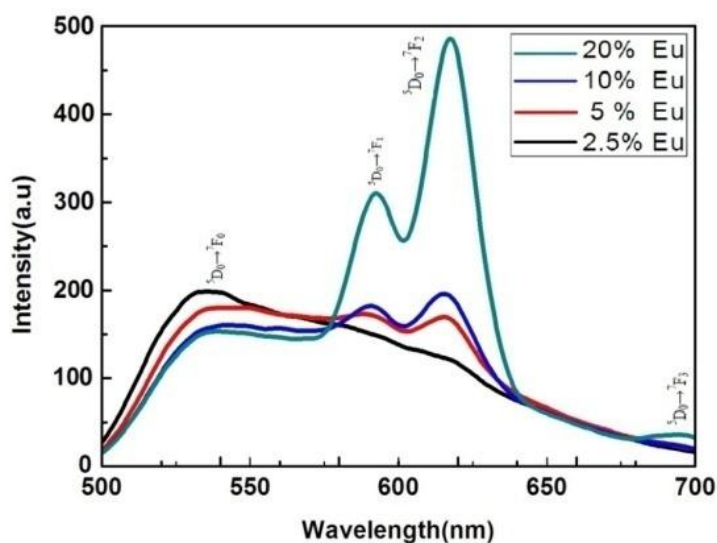


Figure 5. Room temperature fluorescence emission spectra of $\text{ZnO}:\text{Eu}^{3+}$ for various Eu concentrations at indirect excitation at 395nm.

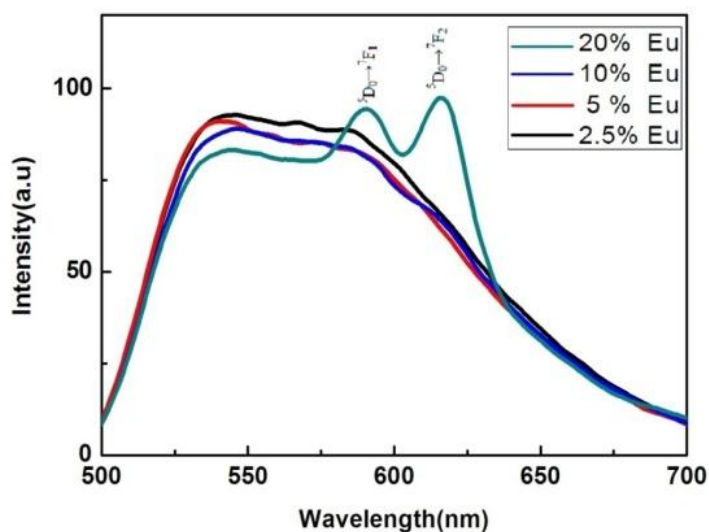


Figure 6. Room temperature fluorescence emission spectra of $\text{ZnO}:\text{Eu}^{3+}$ for various Eu concentrations at direct excitation at 464nm.

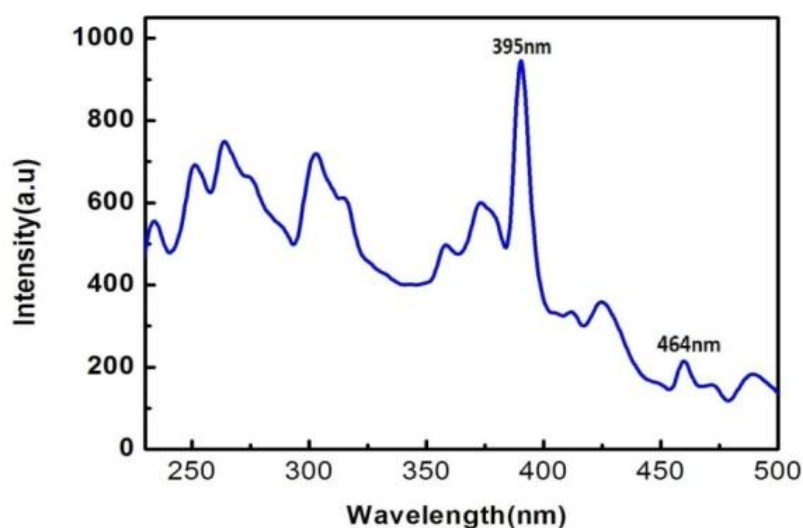


Figure 7. Room temperature phosphorescence excitation spectra of ZnO:5mol%Eu³⁺ for various Eu concentrations at 615 nm.

Figure 10 shows PL spectra of ZnO:Eu³⁺ microspheres with different Eu concentrations under resonantly direct excitation at 464 nm. There are two emission band peaks at 588 nm and 615 nm attributed to ⁵D₀→⁷F₁ and ⁵D₀→⁷F₂ transitions, respectively. The other emissions of Eu³⁺ ions might be partially overlapped by the strong broad defects emission of ZnO matrix from 500 nm to 700 nm. Compared to 395nm indirect excitation, we have observed weak emission peaks under direct excitation at 464 nm. Also, some of weak peaks same as the ⁷F₁→⁵D₁ at 545nm overlapped with broad defects emission. It indicates that, the indirect excitation is more effective than direct excitation due to efficient absorption at UV wavelength in ZnO host and energy transfer to Eu³⁺ ions. This result is against the work of Zhong *et al* [42] that exhibit direct excitation is more effective than indirect excitation.

Since lanthanides emission lifetime is in micro or milliseconds and also weak peaks of Eu ions in fluorescence spectra have been affected by broad defect emission of ZnO, phosphorescence spectroscopy was used for more investigation. Figure 11 shows the room temperature phosphorescence excitation spectra of ZnO: 5

mol%Eu³⁺ monitored at 615 nm. It indicates that indirect excitation at 395nm was more efficient than direct excitation at 464nm.

Figure 12 shows the room temperature phosphorescence emission spectra of Eu-doped ZnO microspheres with different Eu concentrations under indirect excitation at 395nm. It is obvious, with increasing the Eu concentration the intensity of Eu peaks at 588 nm and 615 nm attributed to ⁵D₀→⁷F₁ and ⁵D₀→⁷F₂, respectively, was also enhanced. In phosphorescence spectra, there are two emission peaks at 588nm and 615nm which are attributed to ⁵D₀→⁷F_J (J=1–2) transitions of the Eu³⁺ ions, respectively. ⁵D₀ →⁷F₂ emission arising from an electric-dipole transition results in a large transition probability in crystal fields with inversion anti-symmetry. In addition ⁵D₀→⁷F₁ transition, which originates from a magnetic-dipole transition, shows that Eu³⁺ ions occupy a site with inversion symmetry. The intensity of ⁵D₀→⁷F₂ transition of ZnO:Eu³⁺ sample is stronger than that of ⁵D₀→⁷F₁ transition. This result reveals that due to the larger covalent radius of Eu ions compared with Zn ions, the Eu³⁺ ions are located at a site of inversion antisymmetry in ZnO host.

Figure 13 represents the room temperature phosphorescence emission spectra of Eu-

doped ZnO microspheres with different Eu concentrations under direct excitation at 464nm. At direct excitation at 464nm, which is equal to resonance excitation of photon in ${}^7F_0 \rightarrow {}^5D_2$ transition, red emission intensity was enhanced with increase of Eu concentration. Although in the case of

indirect excitation rather than direct excitation the emission intensity was stronger and more intense due to more energy transfer from host ZnO to Eu^{3+} ions which was consistent with fluorescence spectroscopy result.

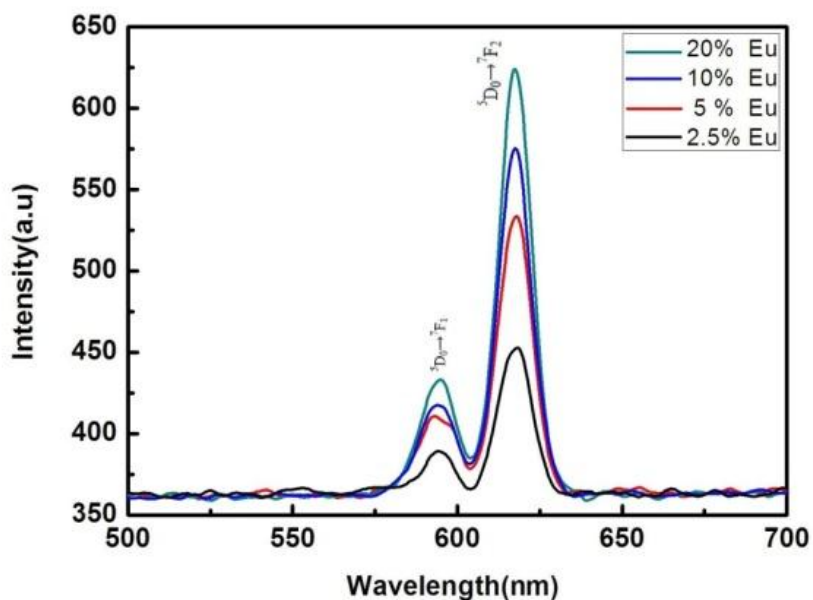


Figure 8. Room temperature phosphorescence emission spectra of $\text{ZnO}:\text{Eu}^{3+}$ for various Eu concentrations in indirect excitation at 395 nm.

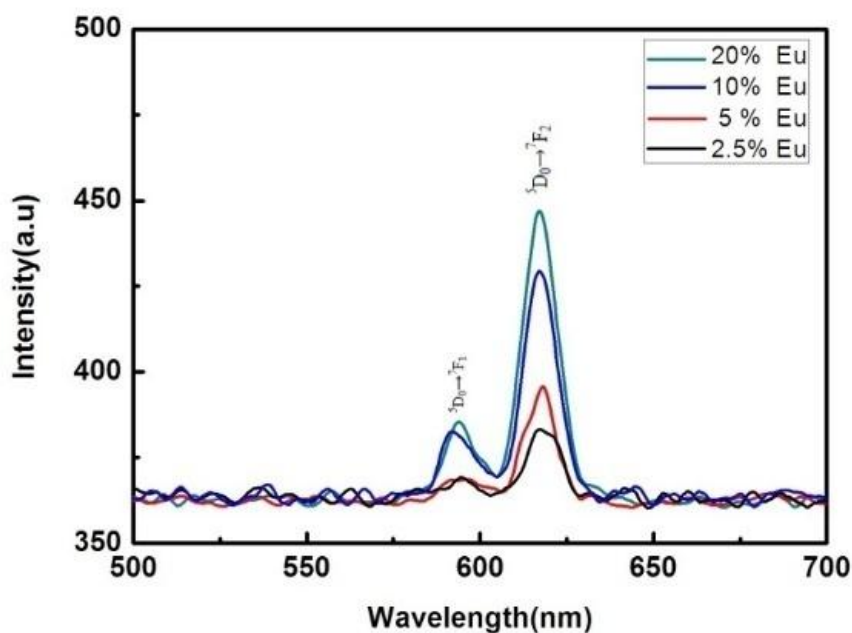


Figure 9. Room temperature phosphorescence emission spectra of $\text{ZnO}:\text{Eu}^{3+}$ for various Eu concentrations at direct excitation at 464 nm.

4. CONCLUSION

In summary, Eu³⁺ doped ZnO microspheres based nano-sheets were synthesized through hydrothermal. Obtain results revealed that ⁵D₀-⁷F₂ emission originated from an electric dipole transition was stronger than other emissions; especially ⁵D₀ → ⁷F₁ emission originated from a magnetic dipole transition. It is suggested that the Eu³⁺ ions mainly take a site with inversion antisymmetry in the ZnO host. PL analysis demonstrated that there was a strong correlation between defect states and red emissions of the Eu³⁺ ions, which shows effective role of intrinsic defects in energy transfer from the ZnO host to the Eu³⁺ ions. The results also showed by increasing Eu concentration, broad defect emission intensity decreased, while Eu intra 4f red emissions intensity enhanced. Comparison of emission intensity in direct and indirect excitation exhibited that indirect excitation is more effective than direct excitation; it represents an efficient absorption process in UV wavelength in ZnO host and energy transfer to Eu³⁺ ions via the intrinsic defect states of ZnO.

REFERENCES

1. J. Song, X. Wang, J. Liu, H. Liu, Y. Li and Z. Wang, *Nano Lett.*, Vol. 8, (2008), pp. 203-207.
2. M. Mehrabian, R. Azimirad, K. Mirabbaszadeh, H. Afarideh and M. Davoudian, *Physica E*, Vol. 43, (2011), pp. 1141-1145.
3. M. D. McCluskey and S. J. Jokela, *J. Appl. Phys.*, Vol. 106, (2009), pp. 71101-71113.
4. A. Ishizumi and Y. Kanemitsu, *Appl. Phys. Lett.*, Vol. 86, (2005), pp. 253106-253112.
5. Y. Liu, W. Luo and R. Li, X. Chen, *Opt. Lett.*, Vol. 32, (2007), pp. 566-568.
6. S. Taguchi, A. Ishizumi, T. Tayagaki and Y. Kanemitsu, *Appl. Phys. Lett.*, Vol. 94, (2009), pp. 173101-173103.
7. Y. K. Park, J. I. Han, M. G. Kwak and et al, *Appl. Phys. Lett.*, Vol. 72, (1998), pp. 668-670.
8. Y.C. Kong, D.P. Yu, B. Zhang, W. Fang and S.Q. Feng, *Appl. Phys. Lett.*, Vol. 78, (2001), pp. 407-409.
9. M. H. Huang, S. Mao, H. Feick, H. Yan, Y. Wu, H. Kind, E. Weber, R. Russo and P. Yang, *Science*, Vol. 292, (2001), pp. 1897-1899.
10. M. H. Huang, Y. Wu, H. Feick, N. Tran, E. Weber and P. Yang, *Adv. Mater.*, Vol. 13, (2001), pp. 113-116.
11. J. Yang, W. Wang, Y. Ma, D.Z. Wang, D. Steeves, B. Kimball and Z.F. Ren, *J. Nanosci. Nanotechnol.*, Vol. 6, (2006), pp. 2196-2199.
12. S.Y. Li, P. Lin, C.Y. Lee and T.Y. Tseng, *J. Appl. Phys.*, Vol. 95, (2004), pp. 3711-3716.
13. O. Akhavan, M. Mehrabian, K. Mirabbaszadeh and R. Azimirad, *J. Phys. D: Appl. Phys.*, Vol. 42, (2009), pp. 225305-225315.
14. M. Guo, P. Diao and S. Cai, *J. Solid State Chem.*, Vol. 178, (2005), pp. 1864-1873.
15. A.B. Hartanto, X. Ning, Y. Nakata and T. Okada, *Appl. Phys., A*, Vol. 78, (2003), pp. 299-301.
16. H. Yan, R. He, J. Pham and P. Yang, *Adv. Mater.*, Vol. 15, (2003), pp. 402-405.
17. Y.B. Li, Y. Bando, T. Sato and K. Kurashima, *Appl. Phys. Lett.*, Vol. 81, (2002), pp. 144-146.
18. M.H. Huang, S. Mao, H. Feick, H. Yan, Y. Wu, H. Kind, E. Weber, R. Russo and P. Yang, *Science*, Vol. 292, (2001), pp. 1897-1899.
19. J. Petersen, C. Brimont, M. Gallart, G. Schmerber and P. Gilliot, *J. Appl. Phys.*, Vol. 107, (2010), pp. 123522-123527.
20. H. Yoon, J. H. Wu, J. H. Min, J. S. Lee and J. S. Ju, *J. Appl. Phys.*, Vol. 111, (2012), 07B523.
21. C. Panatarani, I. W. Lenggoro and K. Okuyama, *J. Phys. Chem. Solids*, Vol. 65, (2004), pp. 1843-1847.

22. T. Pauporte, F. Pelle, B. Viana and P. Aschehoug, *J. Phys. Chem., C*, Vol. 111,(2007),pp. 15427-15432.
23. T. Sasaki, Y. Ebina, Y. Kitami and M. Watanabe, *Phys. Chem B*, Vol. 105,(2001),pp. 6116-6121.
24. T. Sasaki and M. Watanabe, *J. Phys. Chem B*, Vol. 101,(1997),pp. 10159-10161.
25. J. Q. Hu, Y. Bando, J. H. Zhan, Y. B. Li and T. Sekiguchi, *Appl Phys. Lett.*, Vol. 83,(2003),pp. 4414-4416.
26. H. Klug and L. Alexander, Wiley, New York. (1962).
27. M. Yousefi, M. Amiri, R. Azimirad and A. Z. Moshfegh, *J. Electroanal. Chem.*, Vol. 661, (2011),pp. 106–112.
28. T. S. Moss, *Proc. Phys. Soc. B*, Vol. 67,(1954),pp. 775-782.
29. M. Mazilu, N. Tigau and V. Musat, *Opt. Mater.*, Vol. 34,(2012),pp. 1833-1838.
30. M. Pal, U. Pal, J. M. Gracia and J. F. Pérez-Rodríguez, *Nanoscale Res. Lett.*, Vol. 7,(2012),pp. 1-12.
31. F. A. Selim, M. H. Weber, D. Solodovnikov and K. G. Lynn, *Phys. Rev. Lett.*, Vol. 99,(2007),pp. 85502-85506.
32. L. L. Zhang, C. X. Guo, J. G. Chen and J. T. Hu, *Chin. Phys.*, Vol. 14,(2005),pp. 586-590.
33. R. Wu, Y. Yang, S. Cong, Z. Wu, C. Xie, H. Usui, K. Kawaguchi and N. Koshizaki, *Chem. Phys. Lett.*, Vol. 406, (2005),pp. 457-461.
34. Z. Zhang, V. Quemener, C. H. Lin, B. G. Svensson and L. J. Brillson, *Appl. Phys. Lett.*, Vol. 103, (2013),pp. 72107-72115.
35. J. Ji, L. A. Boatner and F. A. Selim, *Appl. Phys. Lett.*, Vol. 105, (2014), pp. 41102-41105.
36. E. H. Khan, M. H. Weber, M. Matthew and M. D. Cluskey, *Phys. Rev. Lett.*, Vol. 111, (2013),pp. 17401-17405.
37. Y. P. Du, Y.W. Zhang, L.D. Sun and C.H. Yan, *J. Phys. Chem. C*, Vol. 112, (2008), pp. 12234-12241.
38. V. Natarajan, M. K. Bhide, A. R. Dhobale, S.V. Godbole, T. K. Seshagiri, A. G. Page and C. H. Lu, *Mater. Res. Bull.*, Vol. 39, (2004), pp. 2065-2075.
39. P. Dorenbos, L. Pierron, L. Dinca, C. V. Eijk, A. K. Harari and B. Viana, *J. Phys. Condens. Matter.*, Vol. 15, (2003), pp. 511-520.
40. K. Ebisawa, T. Okuno and K. Abe, *J. Appl. Phys.*, Vol 47, (2008), pp. 7234-7236.
41. I. Atsushi and K. Yoshihiko, *Appl. Phys. Lett.*, Vol. 86, (2005), pp. 253106-253114.
42. Z. Mingya, S. Guiye, L. Yajun, W. Guorui and L. Yichun, *Mater. Chem. Phys.*, Vol. 106, (2007), pp. 305–309.